Ratchet effect of a dimer with broken friction symmetry in a symmetric potential

Sebastian von Gehlen, Mykhaylo Evstigneev, and Peter Reimann
Fakultät für Physik, Universität Bielefeld, 33615 Bielefeld, Germany
(Received 12 January 2009; published 19 March 2009)

The one-dimensional overdamped Brownian motion of a dimer consisting of two harmonically interacting components is considered. Both components are coupled to the same heat bath and feel the same spatially periodic symmetric potential, whose amplitude is modulated periodically in time. The friction coefficients may differ between dimer components, thus breaking the dynamical symmetry of the system. In the absence of any external bias, a ratchet effect (directed transport) arises generically. Two accurate approximations for the dimer's velocity and diffusion coefficient are obtained for weak and strong couplings. The velocity of the system can be maximized for each direction by adding an optimal amount of noise and by tuning the driving frequency to an optimal value. Furthermore, there exist two optimal coupling strengths at which the velocity is the largest.

DOI: 10.1103/PhysRevE.79.031114 PACS number(s): 05.40.−a, 02.50.Ey, 05.60.−k

I. INTRODUCTION

Fluctuation and dissipation phenomena are of paramount importance with regard to developing and investigating theoretical models of molecular motors [1,2]. The key mechanism of these models that enables the transformation of isotropic thermal noise into average unidirectional motion is the ratchet effect [1–3]. For over a decade it is known experimentally that the internal properties of motor molecules play, if not the decisive, at least a prominent role in the emergence of directed motion in living organisms [4]. These internal properties, their symmetry-breaking and transport generating effects in spite of originally symmetric environments, are addressed by numerous theoretical studies of coupled particle chains [5], arrays [6], and dimers [7–11], to name but a few. Especially dimers are suited to model such systems because of their internal degree of freedom and their simplicity.

A subclass of systems with internally broken symmetry consists of ratchet systems based on inhomogeneous friction. In underdamped systems, friction applied to the internal degree of freedom can lead to self-propulsion [12], even in the absence of an external potential [13]. A macroscopic mechanical device with frictional asymmetry was experimentally realized converting fluctuating motion (actual sound waves) into unidirectional rotation [14]. Another way of enforced frictional inhomogeneity is a space dependent friction coefficient, both for overdamped and underdamped ratchets [15–17]. In nonratcheting systems, sliding friction of dimers on periodic substrates reveals nonlinear velocity dependence and a striking periodic variation with the ratio of dimer length and substrate period [18–20].

In this paper, we introduce a simple one-dimensional model consisting of two elastically coupled Brownian particles with independent friction coefficients in a symmetric flashing potential. This kind of friction asymmetry is different from the two-state systems with protein friction modeling a molecular motor in [21–23], where fluctuations are rectified by means of switching between states of high and low friction in order to account for cyclical attachment to the track (e.g., cell filaments). In our model, the friction coefficients are neither time nor space dependent but fixed quantities generating a nonzero average velocity. We show that the dimer velocity can be maximized with respect to the noise intensity and driving frequency, and that it is maximal at some optimal coupling strength.

II. MODEL

The total energy U of the dimer consists of two parts: a flashing potential representing the interaction of each dimer component with the surface plus the bond energy of the dimer,

$$U(x_1,x_2,t) = [V(x_1) + V(x_2)]f(t) + \frac{\kappa}{2}(x_2 - x_1 - l_0)^2. \quad (1)$$

The surface interaction V is a sinusoidal function with barrier height ΔV and spatial period L,

$$V(x_i) = [1 - \cos(2\pi x_i/L)]\Delta V/2. \quad (2)$$

Both contributions, $V(x_1)$ and $V(x_2)$, are synchronously and periodically switched on and off by a rectangular signal $f(t)=f(t+\tau)$ of periodicity $\tau=\tau_{\mathrm{on}}+\tau_{\mathrm{off}}$. On phases of duration τ_{on} and off phases of duration τ_{off} alternate such that $f(t)=1$ for $n\tau \le t < n\tau+\tau_{\mathrm{on}}$, and $f(t)=0$ for $n\tau+\tau_{\mathrm{on}} \le t < (n+1)\tau$, where $n \in \mathbb{Z}$. The coupling interaction is assumed to be elastic, with spring constant κ and rest length l_0, meaning that there is no internal force acting between the components if $x_2-x_1=l_0$.

The dynamics of the dimer is modeled as overdamped Brownian motion at temperature T, yielding two coupled equations of motion,

$$\eta_i \dot{x}_i(t) = -\partial U(x_1,x_2,t)/\partial x_i + \sqrt{2\eta_i k_B T}\xi_i(t), \quad (3)$$

for $i \in \{1,2\}$. The η_i are the friction coefficients of the respective dimer components, k_B is the Boltzmann constant, and the $\xi_i(t)$ are Gaussian white noises with $\langle \xi_i(t) \rangle = 0$ and $\langle \xi_i(t)\xi_j(s) \rangle = \delta_{ij}\delta(t-s)$, for $i,j \in \{1,2\}$. The ratio of the friction coefficients can be merged into a dimensionless asymmetry parameter α, allowing us to identify

$$\eta := \eta_1 \quad \text{and} \quad \alpha := \eta_2/\eta_1 \quad (4)$$

throughout the rest of the text. For definiteness, we will focus on the case $\alpha \le 1$. In other words, x_1 is the "slow" and x_2 is the "fast" component of the dimer.

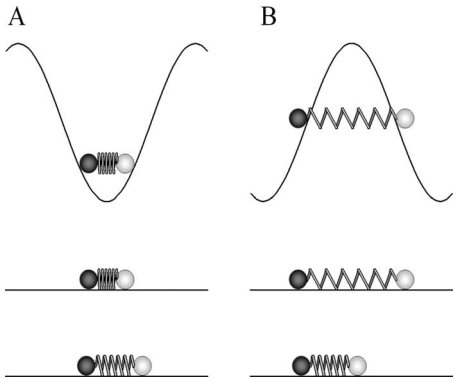

FIG. 1. Schematic representation of two different dimer equilibrium configurations during on phases (dimer plus sinusoidal potential, upper part) and their subsequent deterministic relaxation (off phase, lower part). Dimer constituents are depicted as black (x_1) and white (x_2) balls connected by a spring. For each configuration, a typical relaxation scenario of the dimer is shown for low α values, i.e., x_2 moves faster than x_1. The upper horizontal line represents the initial distribution when the potential V is switched off, the lower line exemplifies the equilibrated spring. The net displacement of the dimer's geometrical center is the origin of the ratchet effect.

The quantities of main interest to us are the average dimer velocity

$$v = \lim_{t\to\infty} \frac{\langle x_i(t)\rangle}{t}, \tag{5}$$

and the diffusion coefficient

$$D = \lim_{t\to\infty} \frac{\langle [x_i(t)]^2\rangle - \langle x_i(t)\rangle^2}{2t}. \tag{6}$$

Focusing on $\kappa > 0$, both quantities are independent of the index i.

III. ORIGIN OF THE RATCHET EFFECT

Before deriving the analytical approximations for the current and diffusion coefficient of the system described in the previous section, we would like to qualitatively discuss the basic mechanisms leading to the onset of a spontaneous current. The origin of the ratchet effect can be understood from Fig. 1, depicting various stages of the dimer's motion.

In each on phase of driving, the dimer may be trapped either (A) near the minimum of the potential $V(x)$, or (B) near its maximum. In case A, the dimer is compressed so that, immediately after the potential $V(x)$ is switched off, the distance between the dimer components will begin to increase toward the equilibrium value l_0. This relaxation will proceed predominantly via the motion of that component, whose friction coefficient is the smaller. As a result, the geometrical center of the dimer will more likely be displaced in the direction of that component in the end of each off phase so that the overall current direction in Fig. 1(A) will be to the right. Turning to case B, the dimer is initially stretched over one of the maxima of the potential $V(x)$. Immediately after this potential is switched off, the dimer length will relax toward the equilibrium value predominantly via the motion of the component with the smaller friction coefficient while the other component will move much more slowly. As a result, the geometrical center will, on average, be displaced to the left in the end of each off phase, resulting in the overall current in the negative direction.

Depending on the rest length and stiffness of the dimer, as well as on the values of the friction coefficient of its components, one of these two scenarios will dominate. At specific values of the system's parameters, both mechanisms can even mutually cancel, resulting in zero net current.

IV. ANALYTICAL DERIVATION OF AVERAGE DIMER VELOCITY AND DIFFUSION COEFFICIENT

The key to a description of the dimer dynamics is a treatment in terms of transition probabilities from distinct potential wells to neighboring wells for the various relevant dimer configurations (e.g., stretched or compressed). However, at a critical coupling strength

$$\kappa_{\mathrm{crit}} := V''(0) = 2\pi^2 \Delta V/L^2, \tag{7}$$

the distinctness of potential minima is severely disturbed by antagonistic superposition of equally strong sinusoidal and elastic parts. It is only for κ well below or above κ_{crit} that we were able to deduce applicable schemes leading to analytical approximations for weak and strong couplings. This can be expressed through the dimensionless parameter

$$\epsilon := \kappa/\kappa_{\mathrm{crit}}, \tag{8}$$

thereby referring to $\epsilon \ll 1$ as weak-coupling regime, and $\epsilon \gg 1$ as strong-coupling regime.

In order to gain analytical results, we need to make three assumptions. The first of them concerns the barrier height. While the periodic driving $f(t)$ of the surface interaction is necessary to drive the dimer out of equilibrium, its amplitude ΔV must be large enough to substantially "freeze" the diffusion in the on phase. Escapes from potential minima must be rare events in order to neglect them completely within an analytical approximation. Therefore, we require

$$\Delta V \gg k_B T. \tag{9}$$

This also guarantees a sharply peaked equilibrium probability distribution of the dimer components whenever the driving is active, $f(t)=1$.

Our second assumption is that τ_{on}, the duration of the surface potential being switched on, must be substantially larger than the relaxation time $\tau_{\mathrm{on}}^{\mathrm{rel}}$ of the slower component x_1,

$$\tau_{\mathrm{on}} \gg \tau_{\mathrm{on}}^{\mathrm{rel}}. \tag{10}$$

Otherwise, the dimer would not reach a quasistationary equilibrium distribution during the on phase. This relaxation time is mainly governed by the curvature of the total potential U at its relative minima. Since the maximal curvature of the potential V equals to κ_{crit}, the relaxation time in the on phase is roughly $\tau_{\mathrm{on}}^{\mathrm{rel}} \sim \eta/(\kappa+\kappa_{\mathrm{crit}})$.

Our third assumption requires that κ is not too small since the spring constant determines the relaxation time $\tau_{\mathrm{off}}^{\mathrm{rel}} = \alpha\eta/(1+\alpha)\kappa$ of the dimer length in the off phase (see below). For

$$\tau_{\text{off}} \gg \tau_{\text{off}}^{\text{rel}}, \tag{11}$$

a lower bound of κ is given by $\kappa \gg \alpha\eta/[(1+\alpha)\tau_{\text{off}}]$ to ensure a stationary equilibrium distribution of the relative coordinate at the end of the off phase.

A. Weak-coupling approximation

Because of conditions (9) and (10), at the end of each on phase, $f(t)=1$, the system finds itself in a sharply peaked equilibrium distribution. Both dimer components will be localized close to minima of $V(x_i)$, say, $x_1 \approx kL$ and $x_2 \approx (k+m)L$, where $k,m \in \mathbb{Z}$. Further, we expect both dimer components to be localized near the positions where $\partial U/\partial x_1 = \partial U/\partial x_2 = 0$, whence we can directly deduce $\sin(2\pi x_1^{\text{eq}}/L) = -\sin(2\pi x_2^{\text{eq}}/L)$ with $x_1^{\text{eq}} + x_2^{\text{eq}} = (2k+m)L$. This means that any equilibrium distribution is completely described by the pair (k,m). By a harmonic approximation of U about $x_1 = kL$ and using $x_2^{\text{eq}} = (2k+m)L - x_1^{\text{eq}}$, the equilibrium positions can be calculated approximately for small ϵ and not too large $|m|$ as

$$x_1^{\text{eq}} = kL + \epsilon(mL - l_0)/(1+2\epsilon), \tag{12}$$

$$x_2^{\text{eq}} = (k+m)L - \epsilon(mL - l_0)/(1+2\epsilon). \tag{13}$$

In the off phase, $f(t)=0$, equation of motion (3) can be decoupled by introducing a dynamically weighted central coordinate,

$$X = (x_1 + \alpha x_2)/(1+\alpha), \tag{14}$$

and a relative coordinate,

$$Y = x_2 - x_1 - l_0. \tag{15}$$

We find for the central coordinate

$$(1+\alpha)\eta\dot{X} = \sqrt{2(1+\alpha)\eta k_B T}\,\xi_X(t), \tag{16}$$

which is a Wiener process, and for the relative coordinate

$$\alpha\eta\dot{Y}/(1+\alpha) = -\kappa Y + \sqrt{2\alpha\eta k_B T/(1+\alpha)}\,\xi_Y(t), \tag{17}$$

being an Ornstein-Uhlenbeck (OU) process. Here, $\xi_X(t)$ and $\xi_Y(t)$ are once again independent delta-correlated Gaussian noises. For initial central coordinate $X^{\text{eq}} = (x_1^{\text{eq}} + \alpha x_2^{\text{eq}})/(1+\alpha)$, see Eqs. (12)–(14), the Wiener process evolves to the probability density

$$W_1(X) = C_X \exp\left(-\frac{(1+\alpha)\eta(X - X^{\text{eq}})^2}{4k_B T \tau_{\text{off}}}\right) \tag{18}$$

in the end of the off phase, where C_X is a normalization constant. Because of condition (11), the OU process approaches its long-time asymptotics

$$W_2(Y) = C_Y \exp(-\kappa Y^2/2k_B T), \tag{19}$$

with a normalization constant C_Y. The joint probability distribution for the original dimer components follows by a backward transformation,

$$\begin{aligned} W(x_1,x_2) &= \int dX\,\delta\left(X - \frac{x_1 + \alpha x_2}{1+\alpha}\right) W_1(X) \\ &\quad \times \int dY\,\delta(Y - x_2 + x_1 + l_0) W_2(Y) \\ &= W_1\left(\frac{x_1 + \alpha x_2}{1+\alpha}\right) W_2(x_2 - x_1 - l_0). \end{aligned} \tag{20}$$

The pair distribution function $W(x_1,x_2)$ is a valid approximation at precisely that moment in time when the potential $V(x_i)$ is switched on again.

Any initial dimer configuration (j,m) can naturally be mapped onto $(0,m)$ by a shift of the coordinate axis by j multiples of L. From there on, the transition probability into any final configuration (k,l) is given by an integral of the pair distribution function,

$$P_{(0,m)\to(k,l)} = \int_{a^-}^{a^+} dx_1 \int_{b^-(x_1)}^{b^+(x_1)} dx_2 W(x_1,x_2). \tag{21}$$

The integration limits, $a^{\pm}$ and $b^{\pm}(x_1)$, must be chosen so as to match the basins of attraction of each minimum, which is a precarious matter for moderately weak coupling. A naive ansatz would be the following: since $\langle Y \rangle = 0$, the elastic part of the potential U can be averaged out and the remaining surface potential $V(x_i)$ leads to $a^{\pm} = (k \pm \frac{1}{2})L$ and $b^{\pm} = (k+l \pm \frac{1}{2})L$. But this rather loose approximation is limited to very small κ and thus is of little use.

Nevertheless, refined approximations of the limits can be established asymptotically both for $\alpha \to 0$ and $\alpha \to 1$. In both cases, we identify $b^{\pm}(x_1)$ with the instantaneous local maximum of $U(x_1,x_2)$ with respect to the variable x_2 for a given value of x_1. Since, in most cases, $\alpha < 1$, the relaxation of the component x_2 then will start toward the accompanying equilibrium closest to $(k+l)L$. Therefore, we determine $b^{\pm}(x_1)$ by expanding $\partial U(x_1,x_2)/\partial x_2$ to first order about $x_2 \approx (k+l \pm \frac{1}{2})L$ and setting it equal to zero, yielding

$$b^{\pm}(x_1) = \frac{\left(k + l \pm \frac{1}{2}\right)L - \epsilon(x_1 + l_0)}{1 - \epsilon}. \tag{22}$$

In a similar manner we wish to determine an effective one-particle potential $\tilde{U}(x_1) = U[x_1, \tilde{x}_2(\alpha)]$ allowing us to deduce the basin of attraction of particle x_1. This must not depend on component x_2 anymore because the integration over x_2 is already completed. Instead of that we introduce a parameter $\tilde{x}_2(\alpha)$ having different meanings in both limits $\alpha \to 0$ and $\alpha \to 1$. In the first case $(\alpha \to 0)$, component x_2 becomes frictionless and will immediately relax to its accompanying equilibrium. This adiabatically accompanying equilibrium is found to be

$$\tilde{x}_2(\alpha = 0) = \frac{(k+l)L + \epsilon(x_1 + l_0)}{1 + \epsilon} \tag{23}$$

by expanding $\partial U(x_1,x_2)/\partial x_2$ to first order about $x_2 \approx (k+l)L$ and setting it equal to zero. In the second case $(\alpha \to 1)$, the relaxation dynamics of both components proceed

on the same time scale. After integrating out the variable x_2, the best estimate we have for $\tilde{x}_2$ is its expectation value in case of x_1 being close to one of its own relative potential maxima at $(k \pm \frac{1}{2})L$. This expectation value is easily calculated to be

$$\tilde{x}_2^{\pm}(\alpha = 1) = \int \int x_2 \delta\left[x_1 - \left(k \pm \frac{1}{2}\right)L\right] W(x_1, x_2) dx_1 dx_2, \tag{24}$$

where the superscript $\pm$ indicates which sign is to be taken at the upper (+) or the lower (−) integration limit.

Now, estimates for the instantaneous boundaries of the basins of attraction for component x_1, denoted by $a_\alpha^{\pm}$, are obtained from an expansion of $\partial \tilde{U}(x_1)/\partial x_1$ at $x_1 \approx (k \pm \frac{1}{2})L$. By using $\tilde{x}_2(\alpha=0)$ within this expansion, we find

$$a_0^{\pm} = \left(k \pm \frac{1}{2}\right)L + \epsilon\left[\left(-l \pm \frac{1}{2}\right)L + l_0\right], \tag{25}$$

and with $\tilde{x}_2^{\pm}(\alpha=1)$ that

$$a_1^{\pm} = a_0^{\pm} + \epsilon[(k+l)L - \tilde{x}_2^{\pm}]/(1+\epsilon). \tag{26}$$

For intermediate α, we choose a linear interpolation for the whole range $0 \leq \alpha \leq 1$ and obtain

$$a^{\pm} = a_0^{\pm} + \alpha(a_1^{\pm} - a_0^{\pm}). \tag{27}$$

With these boundaries, Eq. (21) becomes applicable to all values of α with sufficient accuracy.

At the beginning of a new cycle of driving, the final configuration (k,l) will be mapped onto $(0,m)$, as before. Therefore, we are able to deduce the transition probabilities from initial to final relative distance between components 1 and 2 (i.e., $P_{m\to l}$) via the summation

$$P_{m\to l} = \sum_{k=-\infty}^{\infty} P_{(0,m)\to(k,l)}. \tag{28}$$

These transition probabilities correspond to some stationary nontrivial probability distribution P_m with $\Sigma P_m = 1$ since the matrix elements $P_{m\to l}$ vanish exponentially for large l^2 and m^2. Thus, a formal solution of

$$\sum_{m=-\infty}^{\infty} (P_{m\to l} - \delta_{ml}) P_m = 0, \tag{29}$$

where δ_{ml} is the Kronecker symbol, determines P_m, which are the probabilities of $(0,m)$ states at the beginning of each driving cycle.

For any finite κ, the average velocity of the dimer must be equal to each $\langle \dot{x}_i \rangle$ according to Eq. (5), which by now can be calculated for component x_1 from the transition probabilities $P_{(0,m)\to(k,l)}$. As we are interested in the average shift of x_1 alone, we can first sum over all final l configurations, $\Sigma_l P_{(0,m)\to(k,l)}$. The next step is to sum over all initial m configurations, where the previously determined probabilities P_m enter. Then, after one period of duration τ, each possible step width kL may occur with the assigned probability $\Sigma_{l,m} P_m P_{(0,m)\to(k,l)}$. Finally, the average dimer velocity is obtained by means of a threefold summation,

$$v = \frac{L}{\tau} \sum_k k \sum_m P_m \sum_l P_{(0,m)\to(k,l)}, \tag{30}$$

where all sums run from $-\infty$ to ∞. The diffusion coefficient according to Eq. (6) is obtained from the transition probabilities $P_{(0,m)\to(k,l)}$ in an analogous manner,

$$D = \frac{L^2}{2\tau} \sum_k k^2 \sum_m P_m \sum_l P_{(0,m)\to(k,l)} - \frac{v^2 \tau}{2}. \tag{31}$$

B. Strong-coupling approximation

In the limit of strong coupling, the potential landscape is simplified significantly. In the weak-coupling case considered before, there was a broad variety of "frozen" dimer configurations $(0,m)$ in each on phase, whereas for overcritical κ, there is (in most cases) but a unique equilibrium configuration left. A straightforward but somewhat tedious analysis of the relaxation dynamics on a short time scale leads, for a given ϵ and restricting the rest length l_0 to the interval $[-L/2, L/2]$, to the following approximate upper bound:

$$|l_0| < (L/\pi)\arccos(\sqrt{4\epsilon^2 + 2} - 2\epsilon). \tag{32}$$

Below this bound, any stretched configuration (i.e., dimer components separated by a potential maximum) is always unstable, thus leaving a single stable minimum for any one given x_i.

A further simplification arises from neglecting variations in the relative coordinate Y because of the decreasing width of its distribution function. Since small deviations from the center of this distribution are completely symmetric, their effect cancels in first-order approximation. Therefore it suffices to derive a single parameter transition probability $P_{(0,0)\to(k,0)}$ for the dimer to move by kL as a whole solely from the central coordinate distribution function $W_1(X)$, Eq. (18).

The equilibrium distribution can now be derived by expanding U with respect to x_1, not about kL as before but about $kL - l_0/2$ since this is the correct value in the limit $\epsilon \to \infty$,

$$x_1^{\mathrm{eq}} = kL - \frac{l_0}{2} + \frac{L}{2\pi} \frac{\sin(\pi l_0/L)}{2\epsilon + \cos(\pi l_0/L)}, \tag{33}$$

$$x_2^{\mathrm{eq}} = 2kL - x_1^{\mathrm{eq}}, \tag{34}$$

where $\epsilon \gg 1$ (overcritical coupling). The equilibrium central coordinate that follows from these new values still equals $X^{\mathrm{eq}} = (x_1^{\mathrm{eq}} + \alpha x_2^{\mathrm{eq}})/(1+\alpha)$, yielding for the transition probability the result

$$P_{(0,0)\to(k,0)} = \int_{c^-}^{c^+} dx_1 \int_{-\infty}^{\infty} dX \delta\left(X - x_1 - \frac{\alpha l_0}{1+\alpha}\right) W_1(X). \tag{35}$$

Again, we determine the limits of integration, c^+ and c^-, from the two limiting cases of the asymmetry parameter α. For $\alpha \to 1$, the dimer will settle into that potential well to which its (geometrical) center is the closest. Since we as-

sume $Y \approx 0$, we have $X \approx x_1 + l_0/2$. The dimer therefore will relax to the minimum at kL for $c_1^- < x_1 < c_1^+$, where

$$c_1^{\pm} = \left(k \pm \frac{1}{2}\right)L - l_0/2. \tag{36}$$

In the opposite case $\alpha \to 0$, an expansion of U about $x_1 = (k \pm \frac{1}{2})L - l_0/2$ and using $x_1 + x_2 = (k \pm \frac{1}{2})L$ leads to a basin of attraction of minimum kL between

$$c_0^{\pm} = c_1^{\pm} + \frac{L}{2\pi}\frac{\sin(\pi l_0/L)}{2\epsilon - \cos(\pi l_0/L)}. \tag{37}$$

As before, we choose a linear interpolation for $0 \leq \alpha \leq 1$,

$$c^{\pm} = c_0^{\pm} + \alpha(c_1^{\pm} - c_0^{\pm}). \tag{38}$$

Average dimer velocity and diffusion coefficient follow immediately by adjusting Eqs. (30) and (31), yielding

$$v = \frac{L}{\tau}\sum_k kP_{(0,0)\to(k,0)} \tag{39}$$

and

$$D = \frac{L^2}{2\tau}\sum_k k^2 P_{(0,0)\to(k,0)} - \frac{v^2\tau}{2}. \tag{40}$$

V. RESULTS AND DISCUSSION

To verify the above predictions we compared velocity and diffusion coefficient from Eqs. (30) and (31) in the case of weak coupling, or Eqs. (39) and (40) in the case of strong coupling, to numerical simulations of the original Langevin Eq. (3). Some parameter values were kept fixed throughout all simulations and scaled to unity: thermal energy k_BT, friction coefficient η, and corrugation length L. The barrier height was fixed at $\Delta V = 100 k_B T = 100$ in order to satisfy assumption (9). Also, the duty cycle stayed unaltered, $\tau_{\mathrm{on}}/\tau = 1/2$, dividing the time into equally long on and off phases. Each data point resulted from averaging over 100 trajectories with more than 15 000 duty cycles for undercritical and 1500 for overcritical coupling.

A. Dependence on dimer length

The symmetries of the total energy U naturally depend on the dimer length l_0 through the properties of the elastic part of the potential. Clearly, any U and l_0 dependent quantity, e.g., average dimer velocity, must be affected by those fundamental properties, and we shall discuss these effects briefly. Since the interplay of surface and elastic contributions to total energy U can only be seen during the on phases, $f(t) = 1$, we assume time t to have an appropriate constant value. Therefore, within the subsequent discussion so far t dependence of the potential $U = U(x_1, x_2; t)$ will be abandoned in favor of its dependence on l_0, i.e., from now on $U = U(x_1, x_2; l_0)$.

There are three different symmetry transformations applicable to the spatial variables of U: translational invariance, $U(x_1, x_2; l_0) = U(x_1 + nL, x_2 + ml; l_0 - nL + mL)$, where $n, m \in \mathbb{Z}$,

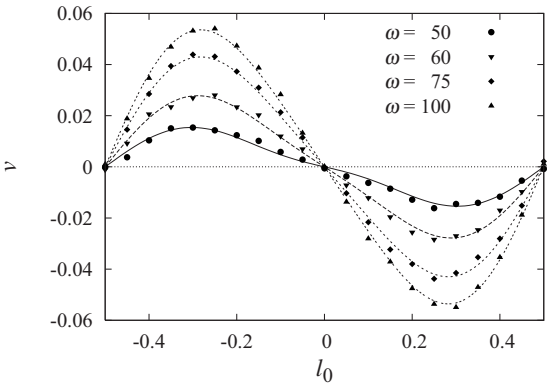

FIG. 2. Average dimer velocity v vs rest length l_0 at four different values of driving frequency $\omega = 50$ (circles and solid line), 60 (downward triangles and long-dashed line), 75 (diamonds and medium dashed line), and 100 (upward triangles and short-dashed line), where $k_BT = \eta = L = 1$, $\alpha = 0.3$, $\Delta V = 100$, and $\kappa = 50$. Data points are taken from simulation data while lines show the corresponding theoretical predictions.

inversion symmetry, $U(x_1, x_2; l_0) = U(-x_1, -x_2; -l_0)$, and exchange symmetry, $U(x_1, x_2; l_0) = U(x_2, x_1; -l_0)$. A change from l_0 to $-l_0$ can be understood as inversion of the dimer's orientation. Necessarily, if the average velocity was nonzero before reorientation, it must be reversed, $v(l_0) = -v(-l_0)$. On the one hand, this immediately implies nodes of $v(l_0)$ at all integer multiples of L due to translation symmetry. On the other hand, translational invariance makes the average velocity a periodic function, $v(l_0) = v(l_0 + kL)$, where $k \in \mathbb{Z}$. Accordingly, we find $v(L/2) = v(-L/2) = -v(L/2)$, which implies nodes of $v(l_0)$ at all half integer multiples of L. Therefore, if v is not constantly zero, it must change its sign in each node at any integer multiple of half the corrugation length, $L/2$. The direction of the average current depends on several parameters and will be discussed in the following sections.

Besides the above mentioned symmetry properties of $v(l_0)$, Fig. 2 includes variations in a further parameter, the driving frequency $\omega = 2\pi/\tau$. Values of ω were chosen from a range well within the bounds imposed by Eqs. (10) and (11). They yield a succession of increasing amplitudes of v, starting from $\omega = 50$ and ending at $\omega = 100$. The abscissa represents the dimer length l_0 and ranges from $-L/2$ to $L/2$, thus covering a single full period of the odd L-periodic function $v(l_0)$. Nodes with change in sign appear at each integer multiple of $L/2$; see explanation above. The absolute value of v exhibits maxima at $|l_0/L| \approx 0.3$. The agreement of theory and simulation within statistical uncertainty is very good for all values depicted.

B. Dependence on friction

The linear interpolation [Eq. (27)] yields accurate results, as can be seen from Fig. 3. Therein, the rest length is a quarter of the spatial period, $l_0 = L/4$, so that velocity $v(l_0)$ is potentially large. For $\alpha = 1$, which means $\eta_1 = \eta_2$, the equations of motion become completely symmetric and the average current must be zero. For decreasing α, the average ve-

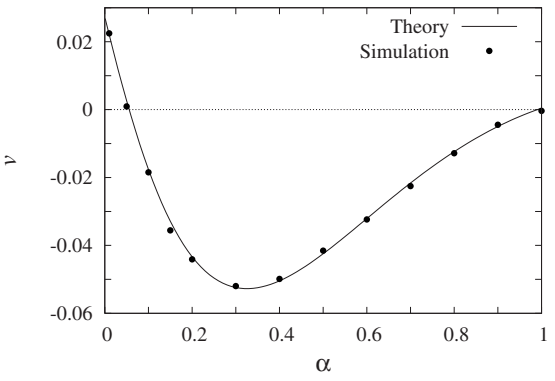

FIG. 3. Dimer velocity v vs asymmetry parameter α, where $\eta = k_B T = L = 1$, $l_0 = 0.25$, $\Delta V = \omega = 100$, and $\kappa = 50$. For $\alpha = 1$, symmetry is restored and the average current is zero; the limit $\alpha \to 0$ means vanishing friction of dimer component x_2 and gives rise to a current reversal.

locity increases until it reaches a maximal absolute value at $\alpha \approx 0.3$. Ongoing decrease in α leads to a current reversal at $\alpha \approx 0.07$ and finally to some finite current in the opposite direction for $\alpha \to 0$.

The qualitative behavior of the velocity v can be explained by two antagonistic effects. The first effect depends on the off-phase equilibrium position of the dimer in the deterministic case; see Fig. 1. At $\alpha = 1$, the whole situation is symmetric with respect to the surface potential. A decrease in α leads to a shift in the final position either to the right (A) or to the left (B), as explained above. For a dimer with rest length $L/4$, as it is the case in Fig. 3, the shift in B is substantially larger than in A, yielding a negative average velocity.

The second effect depends on the shift in the boundaries of integration, i.e., the friction dependent change in the basins of attraction for each dimer component. From simple geometrical reasoning one can deduce that, with $\alpha = 1$ and $l_0 = L/4$, the dimer approximately will end up in A with probability 3/4 and in B with probability 1/4. For $\alpha < 1$, the probability to arrive in a B state is reduced because the fast component x_2 may sometimes pull the slow component x_1 over the top of a potential barrier. This results in a drastic enhancement of the transition probability from any A state into the next A state to the right instead of the B state lying in between. Since the B states have a high transition probability to the left A state, jumps to the left are further decreased for low α. Eventually, with $\alpha \to 0$, the second effect becomes dominating and the average velocity turns to positive values.

C. Dependence on temperature

The vanishing velocity at both extremal temperature limits, see Fig. 4, is readily explained. At zero temperature, the only possible motion is the purely deterministic motion between equilibrium positions of on and off phases; see Fig. 1. This oscillatory motion clearly is bound to a fixed position, generating no net current. At very high temperature, the probability distribution functions of both dimer components become extremely flat. Furthermore, the influence of the surface potential becomes negligible as compared to thermal energy so that the transport generating influence of the driving is substantially reduced.

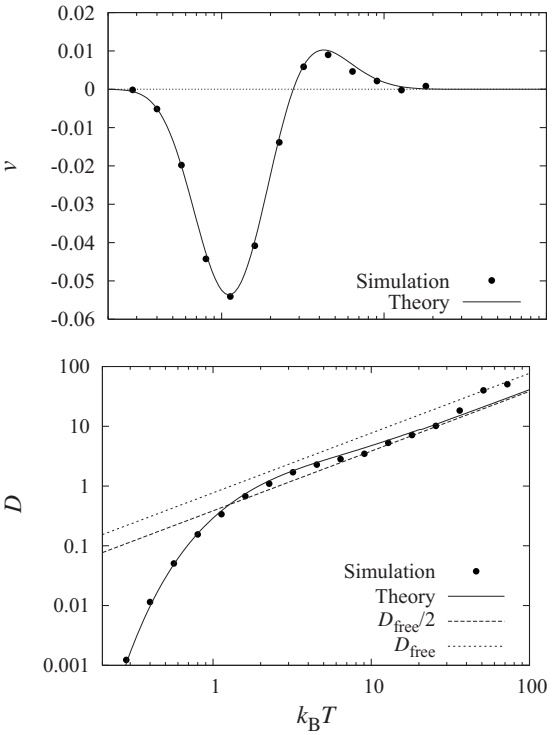

FIG. 4. Dimer velocity v and diffusion coefficient D vs thermal energy $k_B T$, where $\eta = k_B T = L = 1$, $\alpha = 0.3$, $l_0 = 0.25$, $\Delta V = \omega = 100$, and $\kappa = 50$. Upper graph: The velocity shows two extremal values of opposite sign. Lower graph: The coefficient of free diffusion D_{free}, i.e., dimer diffusion without driving, and $D_{\text{free}}/2$ are depicted in dashed lines, as well.

Everything being of physical interest, e.g., a ratchet effect, is to be found in the intermediate temperature regime about $0.1 < k_B T < 100$. The pronounced maximum of negative velocity at $k_B T \approx 1$ and the less prominent maximum of positive velocity at $k_B T \approx 4$ can be explained similarly to the preceding section. When temperature rises from zero, the width of any final off-phase probability distribution grows and transitions into neighboring states become more probable. As long as temperature is low, those widths are rather narrow meaning that any dimer in a B state will proceed to the left A state with high probability. At higher temperature, the transition from a B state to the A state on the right becomes more and more probable, finally leading to a current reversal. Further reversals at still higher temperature could not be observed because assumption (9) is no longer valid.

With regard to the diffusion coefficient, the same temperature ranges reveal different features of the dimer dynamics. For $T \to 0$, the dimer motion becomes subdiffusive since the probability to leave the basin of attraction of a specific state rapidly approaches zero. The free diffusion coefficient of the same dimer but without driving, i.e., with spatially constant surface potential, is $D_{\text{free}} = k_B T/(1+\alpha)\eta$, which is the diffusion coefficient of Wiener process (18). One half of D_{free} is the respective free diffusion coefficient of a dimer that is "frozen" in place according to the same duty cycle

$\tau_{on}/\tau=1/2$ for half of the time but without being relocated to discrete rest positions. At $k_BT\approx 1$, the diffusion coefficient grows larger than $D_{free}/2$, and at $k_BT\approx 4$ it has grown distinctly beyond this value, marking a local maximum of D/D_{free}. This corresponds to the appearance of those transitions that lead directly from an A state to the neighboring A state instead of looping between A and B states. Since this happens while transitions in opposite direction are still important, an ensemble of dimers is tuned toward an optimal mixing. At higher temperatures $(5<k_BT<30)$ this advantage is counterbalanced by the enhancement of transitions from B to the right A state, as explained above, and the diffusion coefficient declines asymptotically to $D_{free}/2$. Finally, for $k_BT\geq\Delta V$, the diffusion becomes quasifree and the coefficient D approaches D_{free}.

D. Dependence on driving frequency

The frequency dependence is related to the temperature dependence of the dimer dynamics via Eq. (18) which has the most decisive influence onto the final result. Therein, thermal energy and duration of the off phase are multiplied to yield the width of the final probability distribution. For duty cycle 1/2, this equals to the ratio of thermal energy and driving frequency according to $k_BT\tau_{on}=\pi k_BT/\omega$. Therefore, one may expect similar results for variation in ω at fixed k_BT as one had for variation in $1/k_BT$ at fixed ω, as long as the assumptions concerning times τ_{on} and τ_{off} are respected.

Regarding velocity, this connection is self-evident from Fig. 5. Starting at low frequency, velocity grows from zero to a first positive maximal value, corresponding to the positive velocity maximum in Fig. 4. Further increase in frequency ω reverts the sign of the net current to a much larger negative velocity, as is the case for decreasing temperature. At even higher frequency, theory disagrees with simulation because assumptions (10) and (11) concerning the relaxation times of dimer components are no longer complied with. The apparent prediction of a second node in the velocity relation therefore lies outside the range of validity; nevertheless the asymptotical decrease in velocity for very high frequency is correct.

The similarity regarding the diffusion coefficient is not so complete because the barrier surmounting effect of very high temperature can only be imitated by such a low frequency that the corresponding large driving period τ entering the denominator of Eq. (31) cancels everything. Therefore a transition from an asymptotic $D_{free}/2$ to a D_{free} regime for $\omega\to 0$ cannot be observed. Instead, in the low-frequency limit analogous to moderately high temperature $(5<k_BT<30)$, there is a saturation of the diffusion coefficient at $D_{free}/2$. Increasing the frequency leads to a clear maximum of diffusivity, above $D_{free}/2$ but still well below D_{free}. The explanation for this maximum of D/D_{free} was given in Sec. V C. This maximum of the diffusion coefficient coincides with the sign reversal of the net current, as well. At high frequency, analogous to low temperature, the time τ_{off} is not long enough to allow for diffusive escape from one of the discrete "rest" states to which the dimer is periodically confined by the surface potential.

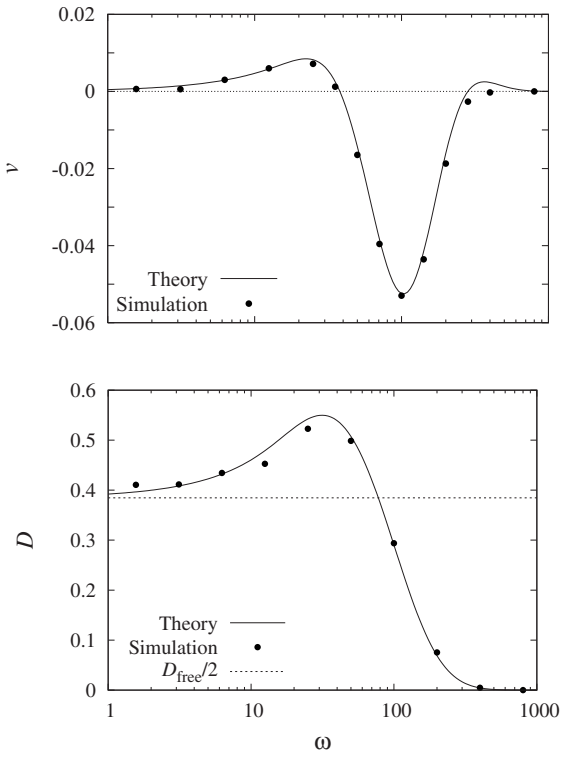

FIG. 5. Dimer velocity v and diffusion coefficient D vs driving frequency $\omega=2\pi/\tau$, where $\eta=k_BT=L=1$, $\alpha=0.3$, $l_0=0.25$, $\Delta V=100$, and $\kappa=50$. Upper graph: The velocity shows two extremal values of opposite sign. The similarity to v as a function of $1/k_BT$ is striking. Lower graph: The maximum of diffusion coincides with the low-ω maximum of v.

E. Dependence on elasticity

As we pointed out in the previous section, the approximation scheme we applied to the dimer dynamics prevents us from any proposition concerning $\kappa\approx\kappa_{crit}$. This particular shortcoming obviously appears in Fig. 6, where there is very good agreement between theory and simulation data in the weak-coupling and the strong-coupling regimes but not at critical coupling where the average dimer velocity is maximized. At this point, both approximations fail completely.

The reasons for the asymptotic behavior of v for weak and strong couplings are clear. In the uncoupled limit $(\kappa\to 0)$, the dimer resolves into two independent particles, each in a symmetric potential that does not yet allow for unidirectional motion. Neither is there any net transport possible in the rigid coupling limit $(\kappa\to\infty)$ because in this case the dynamics can be reduced to the Brownian motion of a single particle (e.g., center of mass) in a symmetric periodic potential. The small positive velocity visible at $\kappa<10$ is a mere artifact. It occurs because assumption (11) concerning the relaxation time in the off phase is violated. If it was desirable to remedy this situation, the stationary probability distribution $W(Y)$ could be replaced by its nonstationary representation.

The internal degree of freedom, Y, becomes physically relevant for finite elasticity only. Similar to Secs. V C and V D, the average velocity possesses two extremal values with different sign. The low-κ maximum (in negative direc-

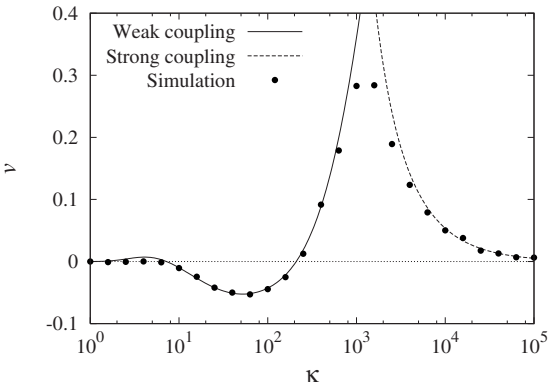

FIG. 6. Dimer velocity v vs elasticity κ, where $\eta=k_BT=L=1$, $\alpha=0.3$, $l_0=0.25$, and $\Delta V=\omega=100$. Weak- and strong-coupling approximations are in good accordance with simulation data over several orders of magnitude of the coupling strength κ. Only at critical coupling, $\kappa^{\mathrm{crit}}\approx 2000$, both approximations fail. In the weak-coupling limit, the average velocity v converges to infinitely small *negative* values, whereas the approximation suggests a small *positive* velocity. This is an artifact due to incomplete relaxation of the dimer, which is not accounted for by our theory.

tion) is captured by the weak-coupling approximation, whereas its high-κ counterpart (in positive direction) coincides with the critical coupling strength. Anyway, both approximations enclose this maximum very tight so that one can easily do without a precise theoretical prediction at κ_{crit}.

Unlike all former results, the maximal velocity in positive x direction is about six times larger than its negative counterpart. There are several reasons for this: the probability of reaching a B state (cf. Fig. 1) with its relaxation into negative direction is diminished because the fast component x_2 can more rigidly pull the slow component x_1 over a potential barrier top. Furthermore, the maximal displacement of A states is increased whereas that of B states is decreased with increasing κ. Last but not least, with further increasing coupling strength, B states become unstable so that a good amount of the probability for traveling backward is lost. Therefore the effect onto the average dimer velocity is by far larger than it was with all previously varied parameters.

VI. CONCLUDING REMARKS

We have investigated the one-dimensional overdamped Brownian motion of a dimer whose elastically coupled components differ in their friction coefficients and are located in a flashing sinusoidal potential. Approximations for the average velocity and diffusion coefficient have been obtained for wide ranges of parameter values, yielding precise theoretical predictions as compared to numerical simulations of the Langevin dynamics. Ratcheting motion has been observed and explained upon variation in rest length, temperature, frictional asymmetry, driving frequency, and elasticity. In each case two parameter values have been found that optimize the velocity, either in positive or in negative direction. For the two most relevant parameters—temperature and frequency—the characteristics of the effective diffusion coefficient have been obtained.

ACKNOWLEDGMENTS

This work was supported by the Deutsche Forschungsgemeinschaft under Grants No. RE 1344/4-1 and No. SFB 613. As part of the European Science Foundation EUROCORES Programme FANAS, it was also supported by the Deutsche Forschungsgemeinschaft and the EC Sixth Framework Programme under Contract No. ERAS-CT-2003-980409.

[1] F. Jülicher, A. Ajdari, and J. Prost, Phys. Rep. **69**, 1269 (1997).
[2] R. D. Astumian, Science **276**, 917 (1997).
[3] P. Reimann, Phys. Rep. **290**, 149 (1997); **361**, 57 (2002).
[4] U. Henningsen and M. Schliwa, Nature (London) **389**, 93 (1997); S. Rice *et al.*, *ibid.* **402**, 778 (1999).
[5] P. Reimann, R. Kawai, C. Van den Broeck, and P. Hänggi, Europhys. Lett. **45**, 545 (1999); C. Van den Broeck, I. Bena, P. Reimann, and J. Lehmann, Ann. Phys. (N.Y.) **9**, 713 (2000).
[6] M. Porto, M. Urbakh, and J. Klafter, Phys. Rev. Lett. **84**, 6058 (2000).
[7] S. Cilla, F. Falo, and L. M. Floria, Phys. Rev. E **63**, 031110 (2001).
[8] S. Klumpp, A. Mielke, and C. Wald, Phys. Rev. E **63**, 031914 (2001).
[9] C. Fusco and A. Fasolino, Thin Solid Films **428**, 34 (2003).
[10] O. M. Braun, R. Ferrando, and G. E. Tommei, Phys. Rev. E **68**, 051101 (2003).
[11] S. von Gehlen, M. Evstigneev, and P. Reimann, Phys. Rev. E **77**, 031136 (2008).
[12] S. Denisov, Phys. Lett. A **296**, 197 (2002).
[13] K. V. Kumar, S. Ramaswamy, and M. Rao, Phys. Rev. E **77**, 020102 (2008).
[14] B. Norden, Y. Zolotaryuk, P. L. Christiansen, and A. V. Zolotaryuk, Phys. Rev. E **65**, 011110 (2001).
[15] D. Dan, M. C. Mahato, and A. M. Jayannavar, Physica A **296**, 375 (2001); Phys. Rev. E **63**, 056307 (2001).
[16] R. Krishnan, D. Dan, and A. M. Jayannavar, Physica A **354**, 171 (2005).
[17] W. L. Reenbohn, S. Saikia, R. Roy, and M. C. Mahato, e-print arXiv:0805.0077.
[18] S. Goncalves, V. M. Kenkre, and A. R. Bishop, Phys. Rev. B **70**, 195415 (2004).
[19] S. Goncalves, C. Fusco, A. R. Bishop, and V. M. Kenkre, Phys. Rev. B **72**, 195418 (2005).
[20] M. Tiwari, S. Gonçalves, and V. M. Kenkre, Eur. Phys. J. B **62**, 459 (2008).
[21] A. Mogilner, M. Mangel, and R. J. Baskin, Phys. Lett. A **237**, 297 (1998).
[22] L. Marrucci, D. Paparo, and M. Kreuzer, J. Phys.: Condens. Matter **13**, 10371 (2001).
[23] H. C. Fogedby, R. Metzler, and A. Svane, Phys. Rev. E **70**, 021905 (2004).